ELSEVIER

Earth and Planetary Science Letters 164 (1998) 467–481

EPSL

Inconsistent magnetic polarities between greigite- and pyrrhotite/magnetite-bearing marine sediments from the Tsailiao-chi section, southwestern Taiwan

Chorng-Shern Horng [a,*], Masayuki Torii [b], Kai-Shuan Shea [c], Shuh-Ji Kao [d]

[a] *Institute of Earth Sciences, Academia Sinica, P.O. Box 1-55, Nankang, Taipei, ROC, Taiwan*
[b] *Department of Biosphere–Geosphere System Science, Okayama University of Science, Okayama, 700-0005, Japan*
[c] *Central Geological Survey, Ministry of Economic Affairs, P.O. Box 968, Taipei, ROC, Taiwan*
[d] *Institute of Oceanography, National Taiwan University, Taipei, ROC, Taiwan*

Received 2 June 1998; revised version received 5 October 1998; accepted 6 October 1998

Abstract

To establish a magnetobiostratigraphy for a 620-m-thick middle to late Pleistocene mudstone sequence in the Lower Gutingkeng Formation of the Tsailiao-chi (TLC) section in southwestern Taiwan, we conducted paleomagnetic and mineral magnetic measurements, together with sediment granulometry and calcareous nannofossil identification. Paleomagnetic samples from 65 sites revealed two types of thermal demagnetization (25–400°C) behavior: (1) single-component stable characteristic remanence in magnetite- and pyrrhotite-dominated samples (Type S), and (2) abrupt changes in polarity when samples with significant greigite concentrations were heated above 320–340°C (Type C). The characteristic polarities derived from Type S samples and from magnetite-dominated Type C samples (obtained above 340°C) are consistent with those determined from nannofossil biostratigraphy. This implies that the NRM carried by magnetite and pyrrhotite is reliable. The essentially antiparallel remanence components in Type C samples below 340°C are attributed to greigite. The almost antiparallel direction could have resulted from delayed formation of greigite, but in this case, the different direction of this component must have resulted from variable remanence lock-in times. Alternatively, the opposite polarities may result from self-reversal, which warrants further investigation. Pyrrhotite and greigite may have both formed authigenically, but there is no clear explanation for the observed differences in direction.

Keywords: magnetostratigraphy; biostratigraphy; Pleistocene; greigite; pyrrhotite; magnetite; Taiwan

1. Introduction

In the past decade, the ferrimagnetic iron sulfides, greigite (Fe_3S_4) and pyrrhotite (Fe_7S_8), have been increasingly reported in sedimentary environments of variable age [1–14]. These two magnetic minerals are usually authigenic products that formed during early diagenesis under anoxic conditions via a complex biogeochemical process of decomposition of organic matter and bacterial sulfate reduction [15–17]. During this process, detrital magnetic iron oxides (e.g., magnetite) will undergo partial or complete dissolution [18]. The formation of magnetic

* Corresponding author. Tel.: +886 2 2783 9910; Fax: +886 2 2783 9871; E-mail: cshorng@earth.sinica.edu.tw

0012-821X/98/$ – see front matter
PII: S0012-821X(98)00239-8

iron sulfides in anoxic environments results in an additional chemical remanent magnetization (CRM), which contributes to the natural remanent magnetization (NRM) of sediments together with the detrital remanent magnetization (DRM) carried by any magnetite that survives dissolution. As a consequence, the coexistence of greigite/pyrrhotite with magnetite in sediments has important implications for paleomagnetism [13,19–23].

In southwestern Taiwan, extraordinarily thick (>3000 m) Plio-Pleistocene marine sequences, which are composed mainly of massive mudstone and muddy siltstone/sandstone, are well exposed along many river sections. In this region, common occurrences of greigite, pyrrhotite and magnetite have been reported in an area of 600 km^2 [7]. The location therefore provides a good opportunity to study the rock magnetic properties of natural greigite/pyrrhotite-bearing sediments [24–26]. This study was aimed at determining the primary remanent component from sediments that are known to contain mixtures of magnetic minerals in order to test the reliability of the paleomagnetic record in sediments whose NRM comprises contributions from DRM and CRM.

2. Geological background and sampling

We sampled the Tsailiao-chi (TLC) river section for magnetobiostratigraphic studies (Fig. 1). This section, located about 25 km east of Tainan City, is truncated by the Tso-chen left-lateral strike-slip fault to the east and is composed of two lithostratigraphic units: the Lower Gutingkeng and the Upper Gutingkeng Formations. These two units belong to a sedimentary sequence that rapidly accumulated since the Pliocene in a subsiding foreland basin [27]. The Lower Gutingkeng Formation is characterized by a dark gray massive mudstone that is intercalated with thin layers of muddy siltstone/sandstone. The Upper Gutingkeng Formation is composed mainly of

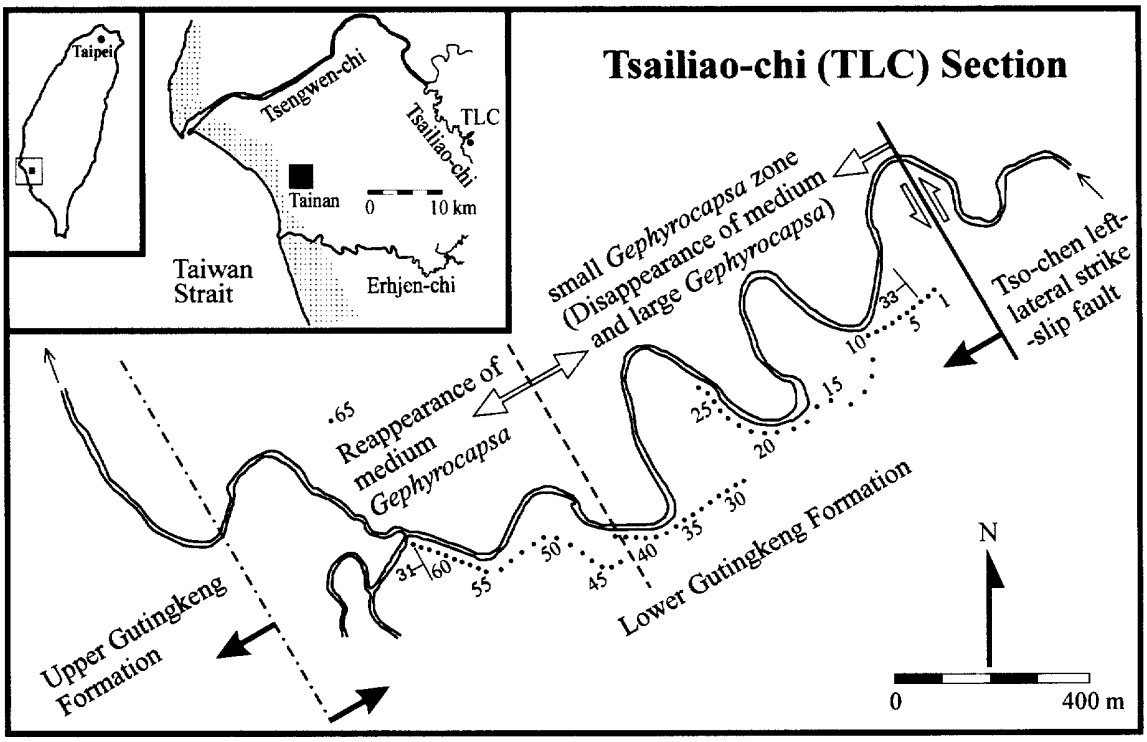

Fig. 1. Map of the TLC section, with location of 65 paleomagnetic sites, lithostratigraphic units and calcareous nannofossil biostratigraphy. The sequence is younger toward the west.

thick layers of muddy siltstone/sandstone. The sequence has a coarsening upward trend. According to a calcareous nannofossil study [28], the age of the section ranges from the middle to late Pleistocene. The reappearance of medium *Gephyrocapsa* occurs in the middle part of the Lower Gutingkeng Formation (Fig. 1) and the interval from this datum level down to the Tso-chen fault is within the small *Gephyrocapsa* zone of Gartner [29], where medium and large *Gephyrocapsa* disappear.

Paleomagnetic sampling was focused on mudstones of the Lower Gutingkeng Formation because fine-grained sediments are usually deposited in a calm environment, which favors preservation of reliable magnetic signals. Cores were oriented (i.e., azimuth and dip) with a mechanical device mounted with a magnetic compass. At each site, about five cores (25 mm in diameter) were drilled after removing the weathered surface of the outcrop. A total of 65 sites were sampled from the 620 m sequence (Fig. 1). Sites were spaced at stratigraphic intervals of 5 to 20 m, depending on exposure.

3. Laboratory procedures

Samples were cut from the oriented cores (22 mm in length) and were subjected to paleomagnetic analysis. Sister samples were used for rock magnetic and low-temperature magnetic measurements. Bulk samples from the same sites were used for magnetic extraction, grain size determination and for identification of calcareous nannofossils.

For the NRM analysis, samples were measured with a 2G Enterprises superconducting rock magnetometer. Thermal demagnetization was conducted with an ASC thermal demagnetizer that has a low field (<10 nT) cooling chamber. The magnetometer and thermal demagnetizer were both situated in a magnetically shielded room. Twelve heating steps from room temperature up to 400°C were employed (i.e., 25, 120, 160, 200, 240, 280, 300, 320, 340, 360, 380 and 400°C). To monitor for changes in magnetic properties, low-field magnetic susceptibility (κ) was measured after each step with a Bartington Instruments MS2 system.

For comparison with thermal demagnetization results, selected sister samples were also treated by thermal demagnetization from 25 to 340°C, and were subsequently subjected to alternating field (AF) demagnetization from 25 to 65 mT with a Molspin AF demagnetizer. Saturation isothermal remanent magnetizations (SIRMs) were imparted to unheated sister samples with an electromagnet (up to fields of 1.1 T). Subsequently, reversed fields were applied in a stepwise manner to determine the coercivity of remanent magnetization (B_{cr}).

Magnetic minerals were extracted from bulk samples (100–200 g) from 24 sites, following the method of Papamarinopoulos et al. [30], and were identified with a Philips X-ray diffractometer (XRD) with CuKα radiation. The morphology of the extracted magnetic minerals was examined with a Hitachi scanning electron microscope (SEM) linked with an energy dispersive X-ray (EDX) analyzer. In addition, the presence of magnetite or pyrrhotite was checked by identifying magnetic phase transitions using low-temperature (5–150 K) magnetic measurements [26,31–33]. The measurements were carried out on small subsamples (~100 mg), using a Quantum Design Magnetic Property Measurement System (MPMS-2). Samples were cooled to 5 K in the MPMS and a 1 T DC field was applied for 10 seconds and the superconducting magnet was then reset to zero. The isothermal remanent magnetizations (IRMs) were measured at one or five degree steps up to 150 K.

Grain size determination was carried out on bulk sediment samples. Relative grain abundances were determined for the following three size fractions, which were separated by mechanical sieving: >63 μm, 45–63 μm, and <45 μm. Smear-slides were examined under a petrographic microscope for nannofossil identification for each site. The slides were prepared following standard procedures [34] and nannofossil ages were determined using the scheme of Berggren et al. [35].

4. Results

4.1. Demagnetization of NRM and nannofossil biostratigraphy

NRM intensities (J_o) and κ_o range between 0.1–39 mA m^{-1} and 182–781 × 10^{-6} (SI), respectively.

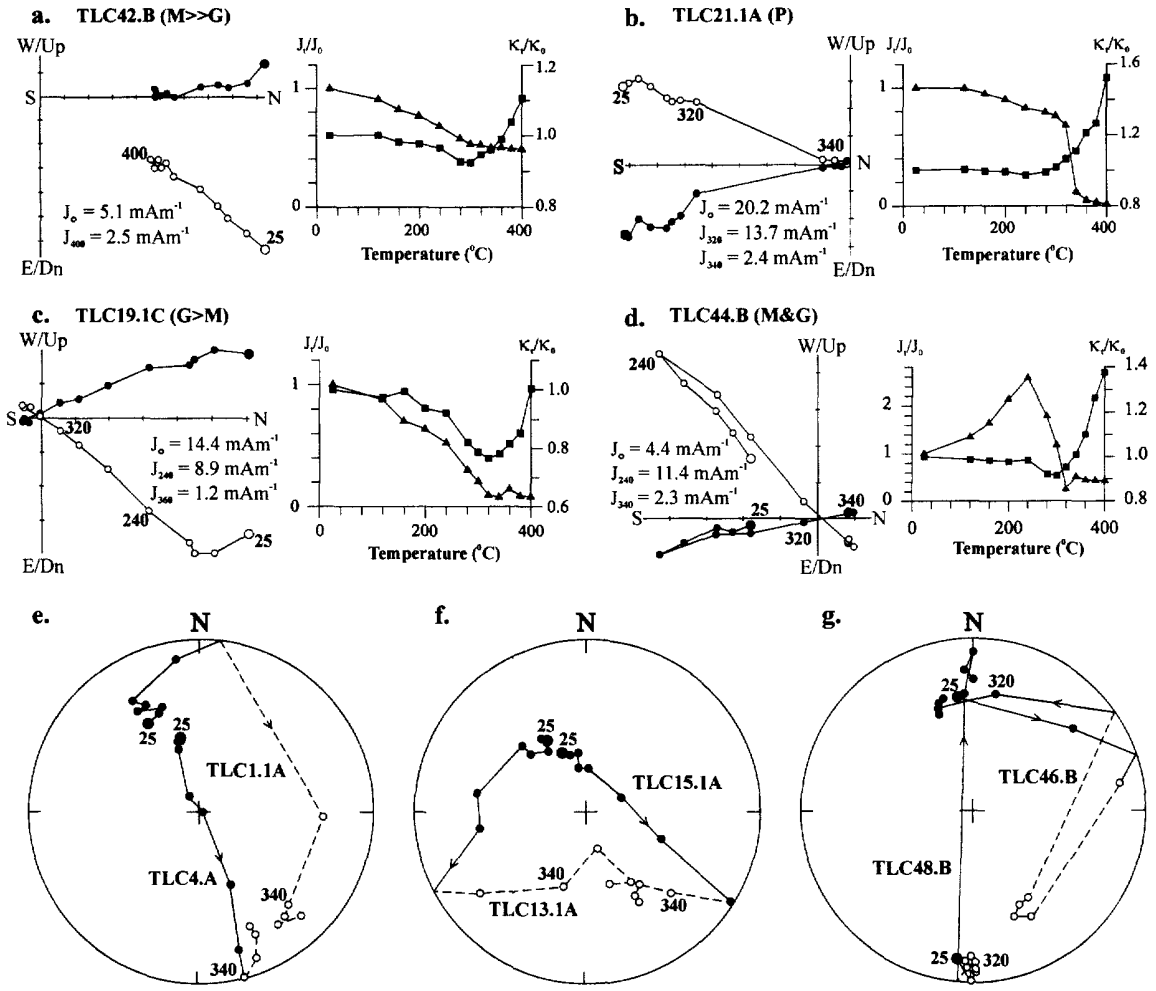

Fig. 2. (a–d) Representative thermal demagnetization diagrams of the TLC samples. The diagrams are after bedding correction (N30°W/30°W). • = horizontal projection; ○ = vertical projection; J_t/J_o (▲) = normalized remanence intensity; κ_t/κ_o (■) = normalized low-field magnetic susceptibility. (a–b) Type S samples carried by dominant magnetite (M) and pyrrhotite (P), respectively. (c–d) Type C samples containing greigite (G) and magnetite (M). (e–g) Representative thermal demagnetization paths of Type C samples on the equal-area projection. • and solid lines = lower hemisphere; ○ and dashed lines = upper hemisphere.

The relatively wide range of these values implies variation in magnetic mineralogy and/or concentration of magnetic particles. In general, thermal demagnetization results are of two contrasting types, designated as Type S (stable) and Type C (changing). The examples shown in Fig. 2 illustrate the two types of behavior. Type S samples have stable characteristic remanence above 240°C (or even below, Fig. 2a, b), whereas Type C samples undergo abrupt changes in magnetic polarity at temperatures around 320–340°C (Fig. 2c–g). The directions obtained after the abrupt change are essentially antiparallel to those before the change. Demagnetization results for two sister samples, which were subjected to thermal demagnetization (25–340°C), followed by AF demagnetization (25–65 mT), are shown in Fig. 3. The results of AF demagnetization are consistent with thermal demagnetization results above 340°C (cf. Fig. 2b, d), which confirms the reliability of high temperature results. Changes in J and κ with tem-

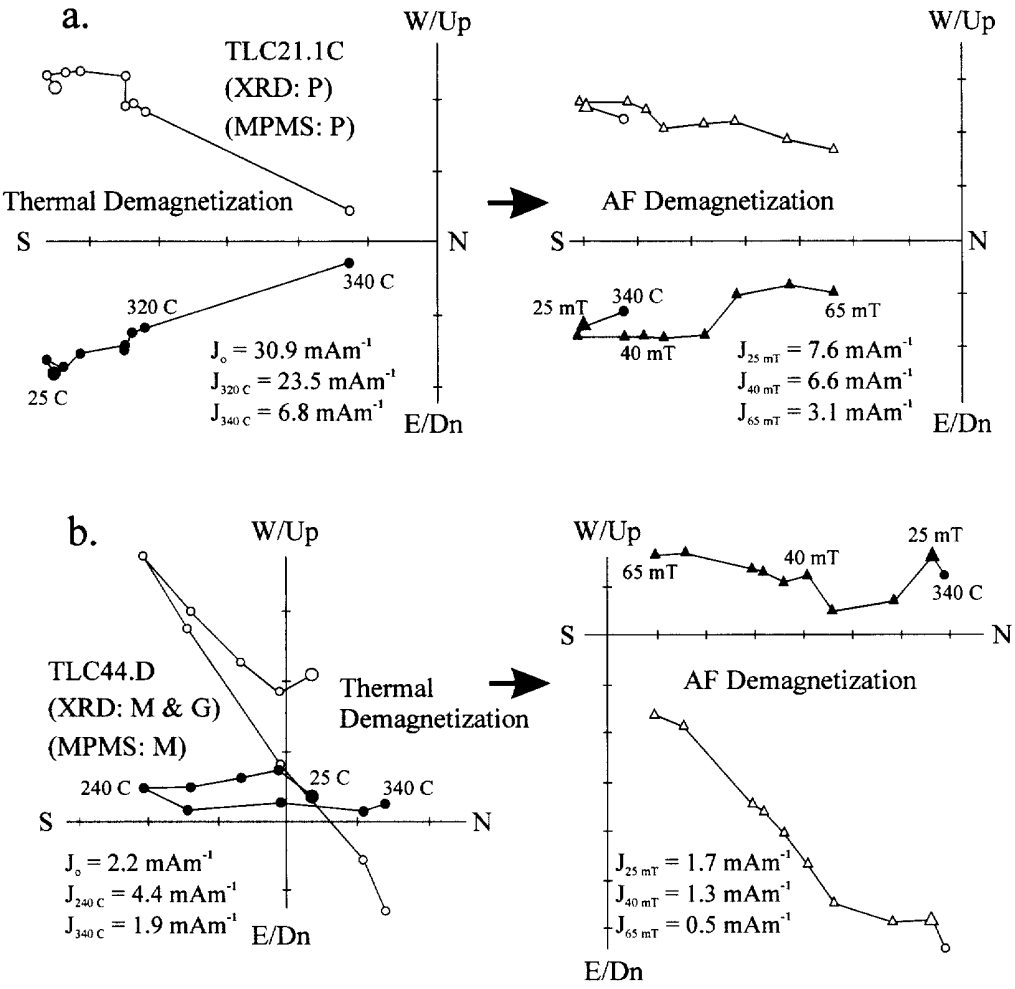

Fig. 3. Thermal and AF demagnetization diagrams for two sets of sister samples. The magnetic minerals (see Table 1) of these two sites are also shown. Thermal demagnetization was carried out from 25 to 340°C (• = horizontal projection; ○ = vertical projection), then AF demagnetization was subsequently applied from 25 to 65 mT (▲ = horizontal projection; △ = vertical projection).

perature are also shown in Fig. 2a–d. Some Type C samples undergo significant decreases in κ at around 240–300°C (e.g., Fig. 2c). Some samples have a different polarity below 240°C to that isolated above 240°C. This behavior is probably attributable to a viscous remanence, which is not further discussed.

For Type C samples, the mean directions of the remanence components isolated between 240–320°C and above 340°C were calculated by line fitting of vector components [36] in orthogonal plots like those shown in Fig. 2c,d. Data obtained from the temperature range below the abrupt polarity change, excluding the inferred viscous remanence component, are referred to as Stage I directions. Data from the temperature range above the abrupt polarity change are referred to as Stage II directions. For Type S samples, a similar calculation was done with the temperature boundary set at 340°C. The results are plotted versus stratigraphic thickness in Fig. 4 and are also shown in equal-area projections in Fig. 5. The polarities based on the mean values of the two stages are presented in Fig. 4 alongside the biostratigraphy defined by calcareous nannofossils. The biostratigraphy indicates that the lower part of the

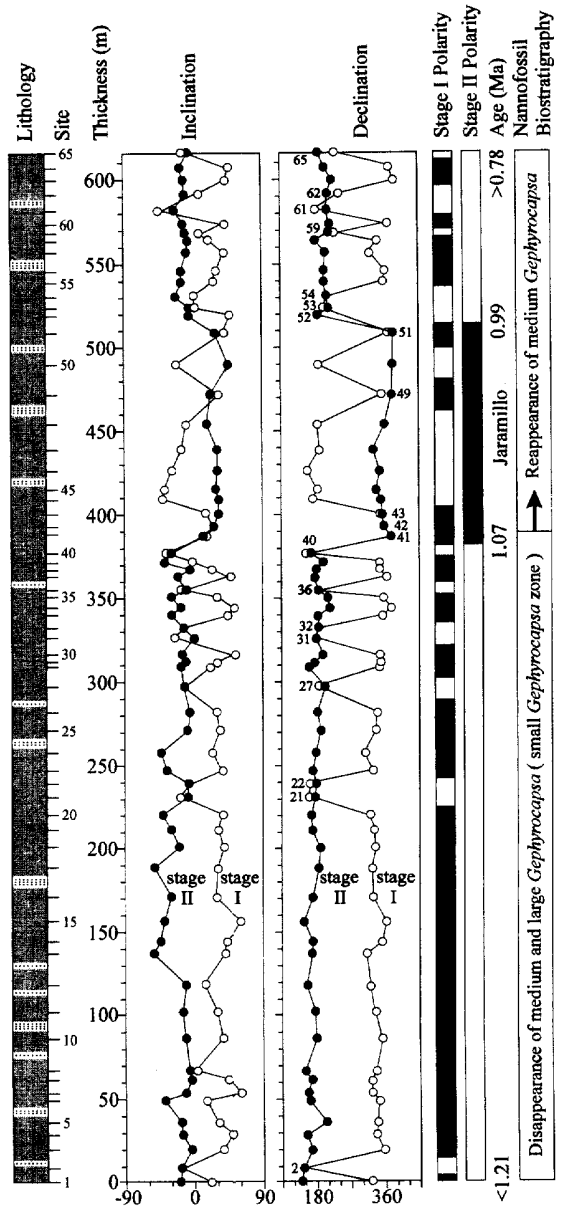

Fig. 4. Stratigraphic plots of declination and inclination of the TLC samples during Stage I and Stage II of thermal demagnetization. Type S sites are denoted with site numbers. The lithology, the polarities of Stage I and Stage II components, the calcareous nannofossil biostratigraphy and the geochronology of Berggren et al. [35] are shown.

sequence (sites 1–41) lies within the small *Gephyrocapsa* zone and that the reappearance of medium *Gephyrocapsa* occurs at site 42 and above.

4.2. Identification and morphology of magnetic minerals

X-ray diffraction analysis (Fig. 6) on magnetic extracts indicates that the samples contain complex assemblages of magnetic minerals, including magnetite (M), pyrrhotite (P) and greigite (G). Their relative concentrations were estimated semi-quantitatively by the intensities of their strongest diffraction peak, as indicated in Table 1. A notable feature is that Type S sites are dominated by magnetite and/or pyrrhotite and that Type C sites are characterized by the coexistence of greigite and magnetite. The occurrences of magnetite and pyrrhotite, as determined from low-temperature measurements (Fig. 7a–d), are consistent with the XRD results, although trace amounts of magnetite below the limit of XRD identification can be detected by low-temperature measurement (Table 1). Consistency between these results indicates that magnetic mineral assemblages determined by XRD are representative of the observed NRM.

The morphologies of the three magnetic minerals under SEM/EDX observation are shown in Fig. 8. Magnetite grains (Fig. 8a) have subangular shapes with numerous dissolution pits. A large titanomagnetite grain (~100 μm, Fig. 8a) has a highly etched surface. However, not all magnetite grains are as large as shown here; some are as small as 3 μm (not shown). These smaller magnetite grains also have etched surfaces. Pyrrhotite grains (Fig. 8b) have tabular hexagon crystals (15–30 μm). In contrast, the morphology of greigite particles (Fig. 8c) is difficult to clearly define due to their small sizes (1–2.5 μm). The greigite particles look like platy hexagons or octahedrons.

4.3. Magnetic properties and lithology

NRM intensity (J_o) and susceptibility (κ_o) of samples before thermal demagnetization are given in Table 1 along with the same properties and SIRM and B_{cr} of the sister samples. Relatively high J_o values (>10 mA m^{-1}) occur in some greigite- and pyrrhotite-dominated samples. However, considerable differences in J_o and κ_o are occasionally observed between sister samples that are dominated by pyrrhotite and/or greigite (e.g., TLC32.1A and TLC32.1B; TLC11.1A and TLC11.1B). SIRM and B_{cr}

Table 1
Summary of magnetic mineralogy, magnetic properties and granulometry of the TLC sediments

Thermal demagnetization samples				Sister samples							Bulk samples		
Thermal demag. samples	J_0 (NRM) (mA m^{-1})	κ_0 (10^{-6} SI)	Polarity	Sister samples	J_0 (NRM) (mA m^{-1})	κ_0 (10^{-6} SI)	SIRM (A m^{-1})	B_{cr} (mT)	SIRM/κ_0 (kA m^{-1})	MPMS	XRD	<45 μm (wt%)	>63 μm (wt%)
Type S thermal demagnetization behavior													
65.1A	0.4	208	R	*65.1B*	0.1	182	0.3	40.7	1.7	–	M	47.0	32.1
54.A	0.9	248	R	*54.B*	1.1	247	0.7	39.2	2.8	–	M	76.2	13.4
43.A	2.0	293	N	*43.B*	1.5	279	1.2	40.7	4.3	M	M	79.6	7.4
42.B	5.1	316	N	*42.C*	4.4	285	1.8	52.0	6.3	–	M≫G	76.4	8.7
40.C	3.4	294	R	*40.B*	2.4	309	7.1	56.5	23.0	–	M	67.2	13.3
61.9A	7.3	304	R	*61.9B*	4.9	293	5.8	44.4	19.8	–	P	86.7	7.1
59.B	1.3	286	R	*59.C*	1.2	275	16.7	39.6	60.7	P≫M	–	–	–
52.A	5.0	261	R	*52.B*	16.4	285	10.8	63.8	37.9	–	P≫G	83.0	5.3
51.A	14.7	309	N	*51.B*	12.4	304	5.5	29.8	18.1	–	P and M	90.8	3.8
36.A	3.6	283	R	*36.B*	3.8	248	0.4	42.6	1.6	P and M	–	85.8	5.9
32.1A	13.0	247	R	*32.1B*	1.5	248	0.8	46.4	3.2	P≫M	P>G	78.9	3.3
31.A	12.4	331	R	*31.B*	24.7	331	14.1	47.6	42.6	–	P	–	–
27.1A	1.7	331	R	*27.1B*	1.9	319	7.3	69.8	22.9	–	P≫G,M	88.5	3.0
22.1A	38.5	296	R	*22.1B*	33.8	299	8.7	43.7	29.1	–	P	82.6	3.4
21.1A	20.2	268	R	*21.1B*	25.0	272	5.4	40.2	19.9	P	P	–	–
Type C thermal demagnetization behavior													
48.B	1.6	293	R–N	*48.C*	0.9	286	2.8	44.5	9.8	–	M and G	94.4	2.5
47.A	0.9	293	R–N	*47.B*	1.3	288	1.6	49.6	5.6	–	M and G	90.1	2.7
46.B	0.7	263	R–N	*46.A*	3.8	296	1.9	42.7	6.4	–	M and G	84.4	4.0
45.A	0.6	305	R–N	*45.B*	2.0	295	1.8	46.4	6.1	–	M and G	90.8	2.7
44.B	4.4	310	R–N	*44.C*	4.4	275	3.9	43.6	14.2	M	M and G	85.9	2.8
19.1C	14.4	436	N–R	*19.1B*	15.0	431	24.7	63.3	57.3	–	G>M	88.7	3.5
11.1A	37.4	781	N–R	*11.1B*	8.1	342	10.8	73.4	31.6	–	G≫M	91.0	3.3
10.B	6.3	368	N–R	*10.C*	1.9	325	5.0	62.0	15.4	M	G and M	92.6	1.7
7.B	19.3	399	N–R	*7.A*	14.6	313	12.1	67.2	38.7	M	G and M	89.0	1.8
5.B	35.5	607	N–R	*5.A*	9.4	464	12.1	75.4	26.1	–	G and M	93.7	2.7
4.A	8.3	357	N–R	*4.B*	7.3	327	9.1	66.7	27.8	–	G and M	–	–

R: reversed polarity; N: normal polarity; M: magnetite; P: pyrrhotite; G: greigite.

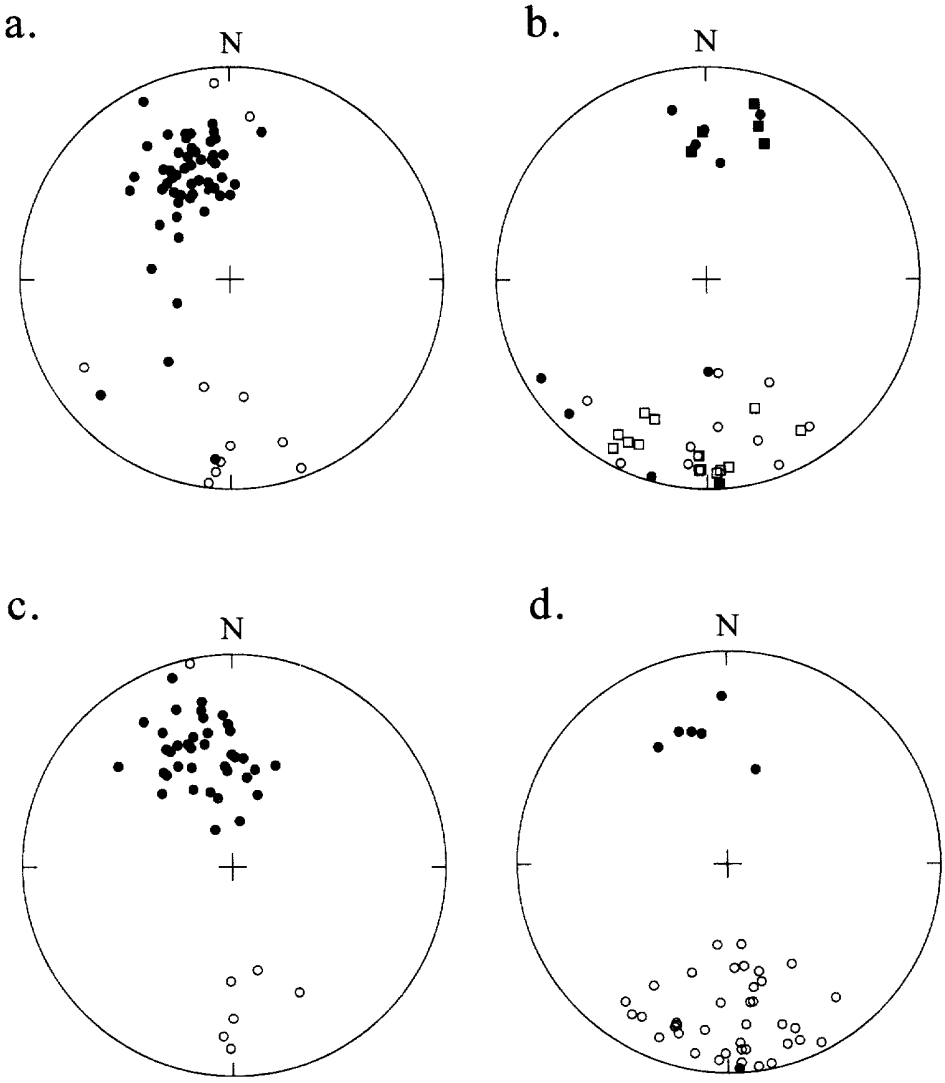

Fig. 5. Equal-area projections of remanence directions for the TLC samples: (a) before demagnetization of the NRM; (b) Stage I (circles) and Stage II (squares) components of Type S samples; (c) Stage I component of Type C samples; and (d) Stage II component of Type C samples. The data in (b), (c), and (d) are from least-squares fits to the data for each component [36]. Solid = lower hemisphere; open = upper hemisphere.

appear to vary with magnetic mineralogy. The greigite-dominated samples have relatively high SIRM (5–24 A m^{-1}) and B_{cr} (62–75 mT), while the magnetite-dominated samples have relatively low SIRM (0.3–7 A m^{-1}) and B_{cr} (39–56 mT).

The grain-size distribution of the sediment is dominated by grains finer than 45 μm in most cases (Table 1). The magnetic mineralogy is related to grain-size distribution, with greigite occurring dominantly in fine-grained sediments (84–94% in the <45 μm fraction). Magnetite is ubiquitous throughout the sequence, but magnetite-dominated samples contain relatively high percentages (7–32%) of coarse grains (>63 μm). Pyrrhotite tends to occur in sediments with grain sizes intermediate between those of greigite-dominated and magnetite-dominated samples.

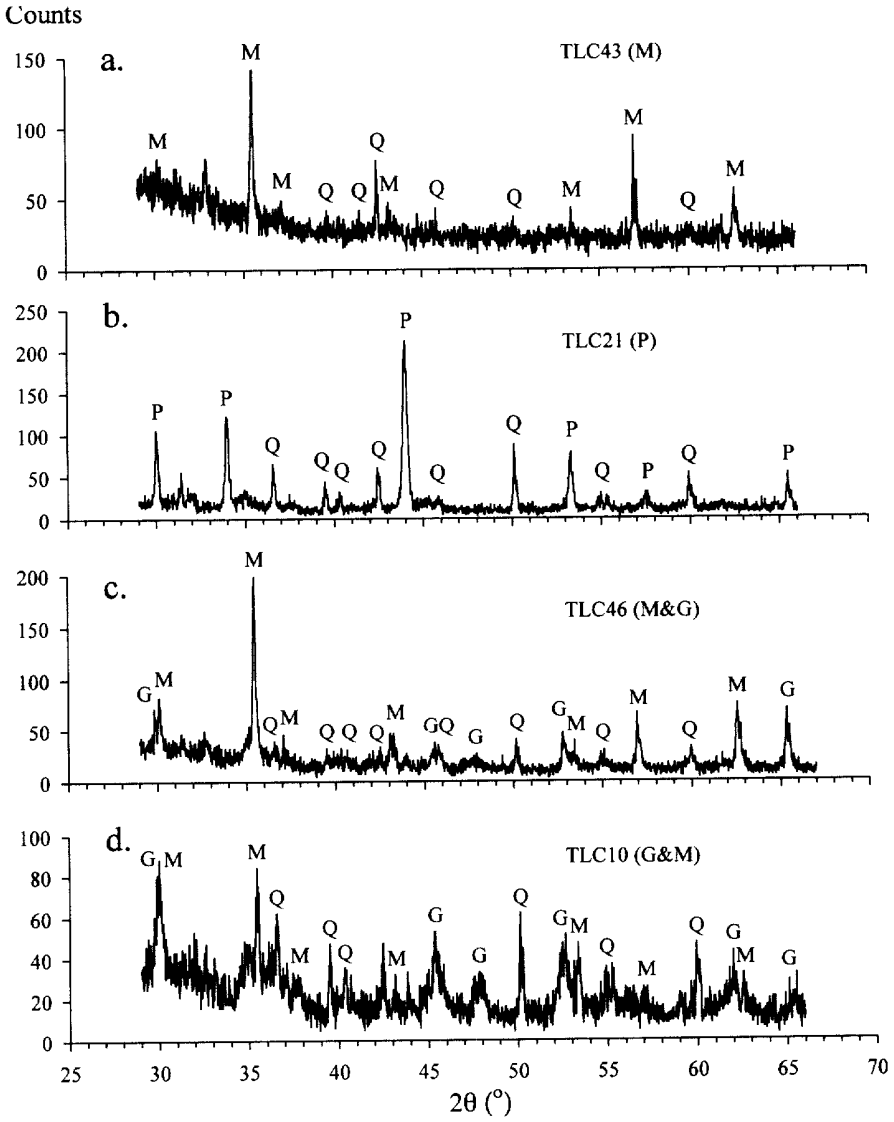

Fig. 6. Representative X-ray diffractograms of magnetic extracts, indicating characteristic peaks of magnetic minerals (Magnetite: *M*, Pyrrhotite: *P*, Greigite: *G*). Quartz (*Q*) generally occurs in the magnetic extracts.

5. Discussion

5.1. Magnetobiostratigraphy

The polarities based on the mean Stage I and Stage II directions are strikingly different (Fig. 4). Samples with consistent polarities (Type S) have magnetic mineral assemblages that are dominated by magnetite and/or pyrrhotite. Those with inconsistent polarities (Type C) all contain significant concentrations of greigite. It is noteworthy that the Stage II polarities of Type C samples are consistent with those of adjacent Type S samples.

According to previous studies [25,26,37], greigite decomposes completely around 330–340°C. This temperature range is close to that at which the abrupt

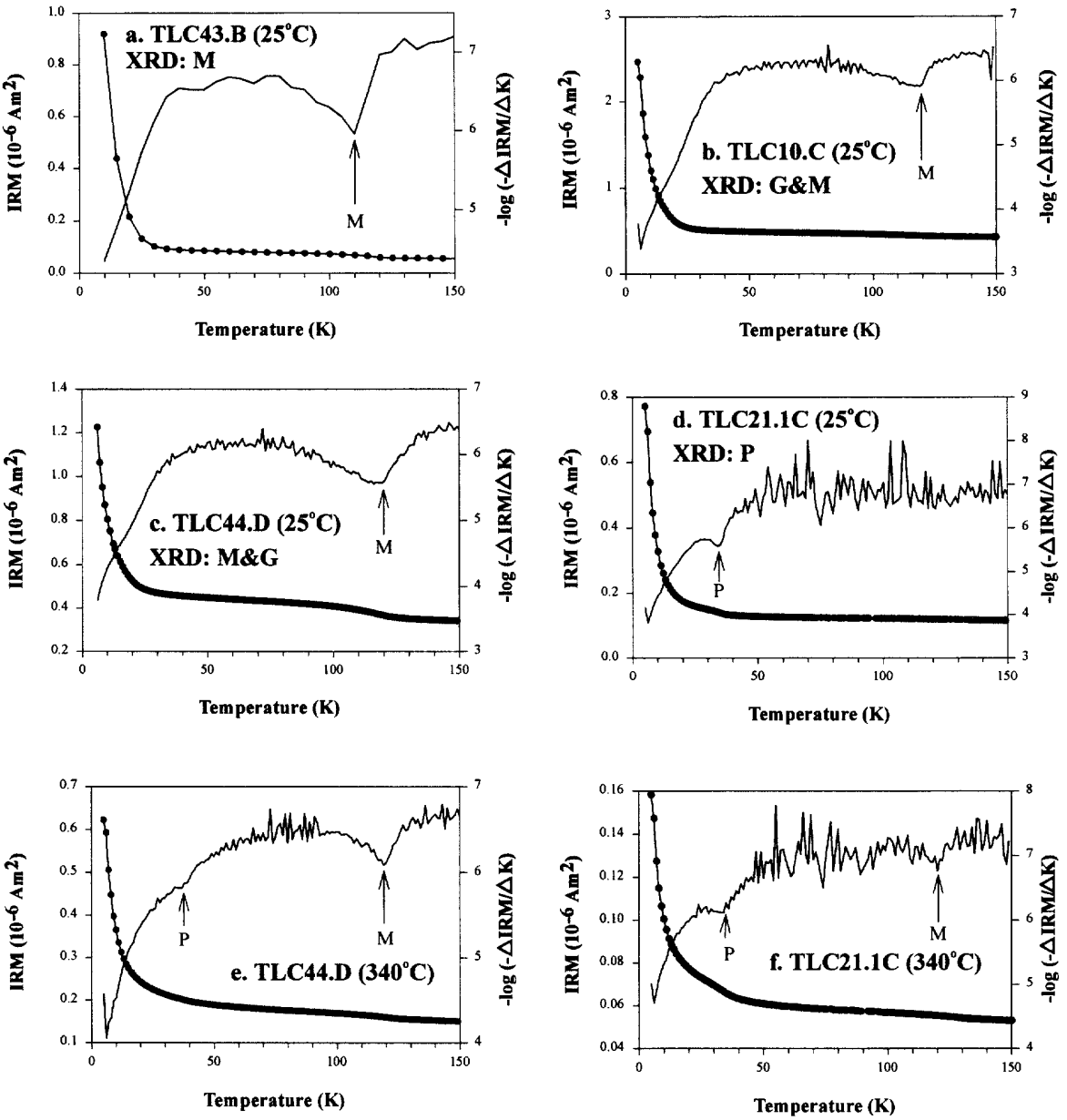

Fig. 7. Low-temperature analysis of IRM (1 T) acquired at 5 K for a small subsample (~100 mg), with measurements made during zero-field warming. The first derivative of the IRM [$-\log(-\Delta\mathrm{IRM}/\Delta K)$] is shown on the right-hand axis to indicate magnetic transitions at 35 K (pyrrhotite: *P*) and 110–120 K (magnetite: *M*) [26,31–33]. Magnetic minerals identified by XRD on magnetic extracts from the same sites are also indicated for each sample. (a–d): Unheated samples. (e–f): after thermal demagnetization at 340°C.

Fig. 8. SEM images of magnetic grains from the TLC magnetic extracts. (a) An octahedral magnetite (*M*) grain (~30 μm) from site 43 has dissolution pits on the surface. A large titanomagnetite (*TM*) grain (~100 μm) on the left reveals a highly etched surface. (b) Pyrrhotite (*P*) crystals (15–30 μm) from site 21, which usually comprise tabular hexagons. (c) Fine-grained greigite (*G*) particles (1–2.5 μm) from site 11. The magnetic grains were identified by EDX chemical analyses after coating with a film of gold (Au).


a
M
870090 20kV X2.00K 15.0um
b
870078 20KV X1.00K 30um
c
870092 20kV X2.00K 4.3um

polarity change is observed among Type C samples. Therefore, it is reasonable to attribute the abrupt polarity change to the removal of the greigite component, which is probably dominant in Type C samples during Stage I. The Stage II remanence of Type C samples must be carried by magnetite that survives thermal decomposition.

The conflicting results observed from the Stage I and Stage II directions can be resolved with the nannofossil biostratigraphy (Fig. 4). The lower part of the sequence is within the small *Gephyrocapsa* zone, which agrees well with the results of Chi and Huang [28]. Based on the datum levels of Berggren et al. [35], this zone defines the age interval from ca 1.21–1.03 Ma, within the Matuyama Chron (Fig. 4). The Stage II remanence directions from sites 1–40 all have reversed polarity, as expected in this Chron. Medium *Gephyrocapsa* reappears at site 42, which is an important datum level in the Jaramillo Subchron [38,39]. According to the biostratigraphy, sites 41 to 51 should be assigned to the Jaramillo Subchron. The Stage II polarities from these sites are all normal. Above site 52, up to site 65, the Stage II remanence has reversed polarity again. Therefore, the polarities based on Stage II data are consistent with that suggested by the biostratigraphy, as are the Stage I results from Type S samples. These results reveal that remanences carried by magnetite and pyrrhotite are reliable for magnetostratigraphic interpretation.

Based on the Stage II polarities and the calcareous nannofossil biostratigraphy, the age of the TLC sequence is unambiguously estimated to be younger than the Cobb Mountain Cryptochron (1.21 Ma) and older than the Matuyama/Brunhes boundary (0.78 Ma) (Fig. 4). The sedimentation rate during this period is estimated to be 1.5–3.0 m/ky, which is of the same order as previously reported [40].

5.2. Origins of the magnetic minerals

The inconsistent polarities exhibited by different magnetic minerals are intriguing and warrant further investigation. The subangular shapes and dissolution pits of the magnetite grains and the highly etched surfaces of titanomagnetite grains (Fig. 8a) provide clear evidence for their detrital origin. These morphological changes result from weathering and diagenetic dissolution (cf. [18]).

Greigite is easily oxidized and its color changes from black to reddish brown during laboratory storage for several months [1,2,11]. It is therefore unlikely that the greigite had a detrital origin. Laboratory experiments have demonstrated that greigite forms as a precursor to pyrite under sulphate-reducing diagenetic conditions [15–17,41] and an authigenic origin for greigite has been inferred in many studies [1–3,8,10–14].

The consistent NRM polarities carried by magnetite and pyrrhotite would imply a similar (i.e., a detrital) origin, but Roberts and Turner [8] suggested an authigenic origin for pyrrhotite in a similar geological setting. Our evidence appears to support an authigenic origin. Some of the pyrrhotite-dominated samples have high values of J_0 (up to 38 mA m^{-1}) and SIRM (up to 16 A m^{-1}), which are similar to those of greigite-dominated samples (Table 1), and unlike the rather low values of magnetite-dominated samples. The SIRM/κ_0 ratio also indicates similarity between pyrrhotite- (mostly between 20–61 kA m^{-1}) and greigite- (15–57 k m^{-1}) dominated samples. The magnetite-dominated samples and their sister samples usually have similar J_0 values, whereas pyrrhotite- or greigite-dominated samples and their sister samples sometimes have rather different J_0 and SIRM values. The difference between sister samples suggests that occurrences of pyrrhotite and greigite are not as homogeneous as magnetite, but are variable on the scale of individual samples.

In contrast to the highly altered morphology of magnetite, the observed morphology of pyrrhotite is euhedral to subhedral (Fig. 8b). If the pyrrhotite grains, which are generally smaller than the magnetite grains, have undergone transport and weathering, they should show more evidence of morphological changes. Moreover, pyrrhotite is found in sediments of a rather narrow range of grain sizes, while magnetite is ubiquitous in the TLC sediments. These observations indicate that the origin of pyrrhotite is similar to that of greigite.

The geochemical conditions under which pyrrhotite is formed during diagenesis are poorly understood except that it can form as an intermediate product under restricted circumstances during pyritization reactions [41]. Laboratory experiments of Sweeney and Kaplan [41] suggested that pyrrhotite may form at low temperature. Roberts and Turner

[8] proposed that preservation of the intermediate products is favored and that pyritization is arrested in fine-grained sediments due to reduced permeability. The TLC sequence was deposited in a similar environment. Within this section, greigite-bearing sediments contain 84 to 94% of fine-grained sediments (<45 μm), while pyrrhotite-bearing sediments contain 79–91% of the <45 μm fraction. The subtle difference in the fine-grained fraction appears to control the occurrence of either greigite or pyrrhotite. This difference may be an indication of the abundance of very fine iron-containing mineral grains that are responsible for the ferrous ion activity in the pore water. This activity may, in turn, control the stability field of pyrrhotite, which exists at a lower ferrous ion activity, or greigite, which exists at a higher ferrous ion activity [42]. Further study is needed to explore this possibility.

The antiparallel remanences carried by greigite and magnetite in Type C samples are perplexing in light of the consistency demonstrated by pyrrhotite and magnetite. One possible explanation for the inconsistency is delayed formation of greigite [13]. For instance, if the greigite remanence at site 1 (Type C), where sediments were deposited at ~1.21 Ma (Fig. 4), was acquired 140 kyr after deposition, its polarity would be normal (Jaramillo) instead of reversed, as expected for the sediment deposition age (Matuyama). If this was the case, the overlying sediments were at least 380 m in thickness when the greigite formed. This is much deeper than was implied (less than 10 m) in the aforementioned case [13] and is much deeper than is expected for greigite formation under normal diagenetic conditions [8]. If greigite was formed at such a great depth, it could have been associated with gas hydrates [43]. Gas hydrates have been detected in modern continental margin sediments off southwestern Taiwan [44]. However, the length of inferred delay in remanence acquisition would change from site to site in order to achieve the apparent antiparallel polarities of greigite in the TLC section, which is difficult to explain. The deep origin of greigite is at odds with observations of greigite formation during early diagenesis in sediments off Taiwan (Horng, unpublished data) as well as in many other places [1–3,6,8–10,12,14,45].

Another possible explanation is self-reversal of greigite [11,13]. The consistently antiparallel polarities of greigite appear to support such an explanation, but the physical mechanism of this hypothetical process is unknown [13].

5.3. Thermal alteration of greigite and pyrrhotite

Greigite and pyrrhotite may change into other forms of magnetic minerals during thermal demagnetization [25,26,37,46]. The newly formed magnetic minerals may acquire a thermal remanent magnetization (TRM) and thereby alter the NRM direction. Determination of magnetic mineralogy before and after thermal demagnetization helps in evaluating the extent of such changes.

Low-temperature measurements of a greigite- and magnetite-bearing sample, which has been demagnetized at 340°C, are shown in Fig. 7e. A weak but clear change in IRM at 35 K suggests that a small amount of pyrrhotite has formed as a result of heating, while magnetite persists. Further thermal demagnetization at temperature above 340°C did not significantly change the directions of remanence, which are consistent with those obtained from AF demagnetization (cf. Fig. 2d, Fig. 3b). Such consistency indicates that thermal alteration has little effect on the NRM direction for samples that contain primary magnetite. In another example (Fig. 7f), magnetite may have formed after thermal demagnetization at 340°C. Its remanent direction remained essentially the same as those observed at lower temperatures (cf. Fig. 2b, Fig. 3a). These results clearly demonstrate that TRM acquisition is insignificant, because the ambient field is well shielded during thermal demagnetization.

6. Conclusions

We identified three magnetic minerals (magnetite, pyrrhotite and greigite) in mudstones throughout the TLC section. Detrital magnetite is ubiquitous, whereas pyrrhotite and greigite occur preferentially in finer-grained sediments. Thermal demagnetization behavior is controlled by the magnetic mineralogy. Magnetite- or pyrrhotite-dominated samples have a stable remanent component above 240°C, and the polarities obtained from these samples are consistent with those determined by nannofossil biostratigraphy. This agreement indicates pyrrhotite to be a

reliable carrier of NRM. By contrast, samples with significant concentrations of greigite exhibit antiparallel remanence directions before total decomposition of greigite around 340°C, while the remanence carried by magnetite at temperatures above 340°C is consistent with polarities expected from biostratigraphy. The reason for the antiparallel directions observed for greigite is not clear. One possibility is due to delayed formation of greigite under special geochemical conditions, but the acquired antiparallel CRM is difficult to explain. Another possibility is due to self-reversal, whose physical mechanism is still unknown.

Although the remanence carried by pyrrhotite is consistent with that of magnetite, the origin of pyrrhotite does not appear to be detrital according to its morphology and magnetic properties. Instead, its origin is probably authigenic, similar to that of greigite. If this is the case, it must have formed rapidly during early diagenesis, but the factors that control the formation of either mineral are not clear.

Acknowledgements

We thank Yi-Chung Yang for helping X-ray analysis, and Sze-How Lee and Rong-Shiang Chang for processing figures and tables. MPMS measurements were done at the low-temperature laboratory of Kyoto University. We gratefully acknowledge Teh-Quei Lee, Chen-Feng You and Yuk-Ling Yung for stimulating this study and reading the manuscript. Andrew Roberts and Kon-Kee Liu are most sincerely thanked for discussions and for improving the paper. Critical comments from Ian Snowball and an anonymous reviewer are invaluable. This study was financially supported by the National Science Council of the Republic of China under grant NSC83-0202-M-001-063 to C.S.H. and M.T. received support from the Superplume Project of the Science and Technology Agency of Japan. *[RV]*

References

[1] R. Snowball, Thompson, The occurrence of greigite in sediments from Loch Lomond, J. Quat. Sci. 3 (2) (1988) 121–125.

[2] R. Snowball, Thompson, A stable chemical remanence in Holocene sediments, J. Geophys. Res. 95 (B4) (1990) 4471–4479.

[3] J. Hilton, Greigite and the magnetic properties of sediments, Limnol. Oceanogr. 35 (2) (1990) 509–520.

[4] M. Krs, M. Krsová, P. Pruner, A. Zeman, F. Novák, J. Jansa, A petromagnetic study of Miocene rocks bearing micro-organic material and the magnetic mineral greigite (Sokolov and Cheb basins, Czechoslovakia), Phys. Earth Planet. Inter. 63 (1990) 98–112.

[5] R.L. Reynolds, N.S. Fishman, R.B. Wanty, M.B. Goldhaber, Iron sulfide minerals at Cement oil field, Oklahoma: Implications for magnetic detection of oil fields, Geol. Soc. Am. Bull. 102 (1990) 368–380.

[6] E. Tric, C. Laj, C. Jéhanno, J.-P. Valet, C. Kissel, A. Mazaud, S. Iaccarino, High-resolution record of the upper Olduvai transition from Po Valley (Italy) sediments: Support for dipolar transition geometry?, Phys. Earth Planet. Inter. 65 (1991) 319–336.

[7] C.-S. Horng, J.-C. Chen, T.-Q. Lee, Variations in magnetic minerals from two Plio-Pleistocene marine-deposited sections, southwestern Taiwan, J. Geol. Soc. China 35 (4) (1992) 323–335.

[8] A.P. Roberts, G.M. Turner, Diagenetic formation of ferrimagnetic iron sulphide minerals in rapidly deposited marine sediments, South Island, New Zealand, Earth Planet. Sci. Lett. 115 (1993) 257–273.

[9] C. Mary, S. Iaccarino, V. Courtillot, J. Besse, D.M. Aissaoui, Magnetostratigraphy of Pliocene sediments from the Stirone river (Po Valley), Geophys. J. Int. 112 (1993) 359–380.

[10] R.L. Reynolds, M.L. Tuttle, C.A. Rice, N.S. Fishman, J.A. Karachewski, D.M. Sherman, Magnetization and geochemistry of greigite-bearing Cretaceous strata, North Slope basin, Alaska, Am. J. Sci. 294 (1994) 485–528.

[11] D.F. Hallam, B.A. Maher, A record of reversed polarity carried by the iron sulphide greigite in British early Pleistocene sediments, Earth Planet. Sci. Lett. 121 (1994) 71–80.

[12] C.H. Lee, J.-H. Jin, Authigenic greigite in mud from the continental shelf of the Yellow sea, off the southwest Korean Peninsula, Mar. Geol. 128 (1995) 11–15.

[13] F. Florindo, L. Sagnotti, Palaeomagnetism and rock magnetism in the upper Pliocene Valle Ricca (Rome, Italy) section, Geophys. J. Int. 123 (1995) 340–354.

[14] A.P. Roberts, R.L. Reynolds, K.L. Verosub, D.P. Adam, Environmental magnetic implications of greigite (Fe_3S_4) formation in a 3 m.y. lake sediment record from Butte Valley, northern California, Geophys. Res. Lett. 23 (20) (1996) 2859–2862.

[15] M.B. Goldhaber, I.R. Kaplan, The sulfur cycle, in: E.D. Goldberg (Ed.), The Sea, Marine Chemistry, vol. 5, Wiley, New York, 1974, pp. 569–655.

[16] B.B. Jørgenson, The sulfur cycle of a coastal marine sediment (Limfjorden, Denmark), Limnol. Oceanogr. 22 (5) (1977) 814–832.

[17] R.A. Berner, Thermodynamic stability of sedimentary iron sulfides, Am. J. Sci. 265 (1967) 773–785.
[18] D.E. Canfield, R.A. Berner, Dissolution and pyritization of magnetite in anoxic marine sediments, Geochim. Cosmochim. Acta 51 (1987) 645–659.
[19] F. Giovanoli, A comparison of the magnetization of detrital and chemical sediments from Lake Zurich, Geophys. Res. Lett. 6 (4) (1979) 233–235.
[20] S.P. Lund, R. Karlin, Introduction to the special section on physical and biogeochemical processes responsible for the magnetization of sediments, J. Geophys. Res. 95 (B4) (1990) 4353–4354.
[21] A.A.M. van Hoof, C.G. Langereis, Reversal records in marine marls and delayed acquisition of remanent magnetization, Nature 351 (1991) 223–225.
[22] K.L. Verosub, A.P. Roberts, Environmental magnetism: Past, present and future, J. Geophys. Res. 100 (B2) (1995) 2175–2192.
[23] I.F. Snowball, Gyroremanent magnetization and the magnetic properties of greigite-bearing clays in southern Sweden, Geophys. J. Int. 129 (1997) 624–636.
[24] C.-S. Horng, C. Laj, T.-Q. Lee, J.-C. Chen, Magnetic characteristics of sedimentary rocks from the Tsengwen-chi and Erhjen-chi sections in southwestern Taiwan, TAO 3 (4) (1992) 519–532.
[25] A.P. Roberts, Magnetic properties of sedimentary greigite (Fe_3S_4), Earth Planet. Sci. Lett. 134 (1995) 227–236.
[26] M. Torii, K. Fukuma, C.-S. Horng, T.-Q. Lee, Magnetic discrimination of pyrrhotite- and greigite-bearing sediment samples, Geophys. Res. Lett. 23 (14) (1996) 1813–1816.
[27] M. Covey, The evolution of foreland basins to steady state: Evidence from the western Taiwan foreland basin, in: P.A. Allen, P. Homewood (Eds.), Foreland Basins, Spec. Publ. Int. Assoc. Sedimentol. 8 (1986) 77–90.
[28] W.-R. Chi, H.-M. Huang, Nannofossil biostratigraphy of sediments of the Chiutsenglin anticline, Tainan area, Bull. Explor. Develop. Res. Center, Chinese Petrol. Corp. 17 (1983) 39–56 (in Chinese with English abstract).
[29] S. Gartner, Calcareous nannofossil biostratigraphy and revised zonation of the Pleistocene, Mar. Micropaleontol. 2 (1977) 1–25.
[30] S. Papamarinopoulos, P.W. Readman, Y. Maniatis, A. Simopoulos, Magnetic characterization and Mössbauer spectroscopy of magnetic concentrates from Greek lake sediments, Earth Planet. Sci. Lett. 57 (1982) 173–181.
[31] M.J. Dekkers, J.-L. Mattéi, G. Fillion, P. Rochette, Grain-size dependence of the magnetic behavior of pyrrhotite during its low-temperature transition at 34 K, Geophys. Res. Lett. 16 (8) (1989) 855–858.
[32] P. Rochette, G. Fillion, J.-L. Mattéi, M.J. Dekkers, Magnetic transition at 30–34 Kelvin in pyrrhotite: insight into a widespread occurrence of this mineral in rocks, Earth Planet. Sci. Lett. 98 (1990) 319–328.
[33] Ö. Özdemir, D.J. Dunlop, B.M. Moskowitz, The effect of oxidation on the Verwey transition in magnetite, Geophys. Res. Lett. 20 (16) (1993) 1671–1674.
[34] K. Perch-Nielsen, Mesozoic calcareous nannofossils, in: H.M. Bolli, J.B. Saunders, K. Perch-Nielsen (Eds.), Plankton Stratigraphy, Cambridge Univ. Press, 1985, pp. 329–426.
[35] W.A. Berggren, F.J. Hilgen, C.G. Langereis, D.V. Kent, J.D. Obradovich, I. Raffi, M.E. Raymo, N.J. Shackleton, Late Neogene chronology: New perspectives in high-resolution stratigraphy, Geol. Soc. Am. Bull. 107 (11) (1995) 1272–1287.
[36] J.L. Kirschvink, The least-squares line and plane and the analysis of paleomagnetic data, Geophys. J. R. Astron. Soc. 62 (1980) 699–718.
[37] M. Krs, F. Novák, M. Krsová, P. Pruner, L. Koukílková, J. Jansa, Magnetic properties and metastability of greigite–smythite mineralization in brown-coal basins of the Krusné hory Piedmont, Bohemia, Phys. Earth Planet. Inter. 70 (1992) 273–287.
[38] H. Matsuoka, H. Okada, Quantitative analysis of Quaternary nannoplankton in the subtropical northwestern Pacific Ocean, Mar. Micropaleontol. 14 (1989) 97–118.
[39] W. Wei, Calibration of upper Pliocene–lower Pleistocene nannofossil events with oxygen isotope stratigraphy, Paleoceanography 8 (1) (1993) 85–99.
[40] S.S.L. Chang, W.-R. Chi, Neogene nannoplankton biostratigraphy in Taiwan and the tectonic implications, Petrol. Geol. Taiwan 19 (1983) 93–147.
[41] R.E. Sweeney, I.R. Kaplan, Pyrite framboid formation: Laboratory synthesis and marine sediments, Econ. Geol. 68 (5) (1973) 618–634.
[42] C.J. Lord III, T.M. Church, The geochemistry of salt marshes: Sedimentary iron diffusion, sulfate reduction, and pyritization, Geochim. Cosmochim. Acta 47 (1983) 1381–1391.
[43] B.A. Housen, R.J. Musgrave, Rock-magnetic signature of gas hydrates in accretionary prism sediments, Earth Planet. Sci. Lett. 139 (1996) 509–519.
[44] W.-C. Chi, D.L. Reed, C.-S. Liu, N. Lundberg, Distribution of the bottom-simulating reflector in the offshore Taiwan collision zone, TAO 9(4) (1998) in press.
[45] A. Demitrack, A search for bacterial magnetite in the sediments of Eel Marsh, Woods Hole, Massachusetts, in: J.L. Kirschvink, D.S. Jones, B.J. MacFadden (Eds.), Magnetite Biomineralization and Magnetoreception in Organisms, Topics in Geobiology 5, 1985, Plenum Press, New York, pp. 625–645.
[46] M.J. Dekkers, Magnetic monitoring of pyrrhotite alteration during thermal demagnetization, Geophys. Res. Lett. 17 (6) (1990) 779–782.